JOURNAL OF Materials CHEMISTRY

Redox energetics of perovskite-related oxides

Egil Bakken, Truls Norby and Svein Stølen*

Department of Chemistry, University of Oslo, Postbox 1033, N0315 Oslo, Norway. Tel: +47 22 85 56 01; Fax: +47 22 85 54 41; E-mail: svein.stolen@kjemi.uio.no

Received 19th July 2001, Accepted 25th October 2001
First published as an Advance Article on the web 19th December 2001

The present paper focuses on the redox properties of perovskite-related oxides and presents a solution model that connects integral thermodynamic properties that are measured calorimetrically with partial thermodynamic quantities that are measured by equilibration methods. The model allows us to extract significant features of the redox energetics of non-stoichiometric oxides. It is shown that the redox behavior, *e.g.* the composition–partial-pressure isotherms, is independent of the stability of the non-stoichiometric oxides and as a first approximation is directly given by the relative stability of the oxidation states involved. The stability of a given oxidation state is related to the structure of the oxide, and the large difference in redox behavior between hexagonal and cubic $SrMnO_{3-\delta}$ is rationalized. Whereas both the enthalpy and entropy of oxidation in general depend on temperature, a number of systems can be adequately described using an ideal solution approach. This implies that composition-independent enthalpic and entropic terms can be used as first approximations to describe the redox energetics of non-stoichiometric oxides. In order to illustrate the approach an overview of the redox energetics of selected $La_{1-x}Ae_xMO_{3-\delta}$ phases (Ae alkaline earth, M transition metal) of interest in connection with solid oxide fuel cell and gas separation membrane applications is given.

Introduction

The interest in perovskite-type and related oxides with variable formal oxidation state of the metals is large. Practical uses of these materials are in many cases related to the variable oxidation state of the metal that is important for, for example, catalytic activity, superconductivity, and mixed ionic and electronic conductivity. The redox properties of non-stoichiometric oxides depend in general on the enthalpy and entropy of oxidation and their variation with composition and temperature. Owing to the large number of factors involved it is in general not straightforward to extract energetic parameters from (stoichiometry, *P*, *T*)-data. Often the interpretations of such data are based on one or more simultaneous point defect equilibria whereas the energetic parameters connected to each of the equilibria are assumed to be independent of composition and temperature.

The thermodynamics of redox reactions in solid oxides can be studied by several different techniques. Most often, the composition of the oxide is determined as a function of the partial pressure of oxygen and temperature and the energetics of the redox reactions deduced from the variation of the equilibrium P_{O_2} with composition.[1,2] Alternatively, calorimetric determinations of enthalpies of oxidation can be made.[3,4] The relationship between calorimetrically determined enthalpies of oxidation and (stoichiometry, *P*, *T*)-relationships is, however, not obvious and the fact that energetic parameters deduced from equilibration studies are often not in agreement with calorimetrically determined quantities is thus not easily addressed. The present paper focuses on the redox properties of perovskite-related oxides and presents a solution model that connects integral thermodynamic properties that are measured calorimetrically with partial thermodynamic quantities that are measured by equilibration methods. The physical implications of the model are discussed, as are enthalpic and entropic contributions to the redox energetics.

Solution thermodynamics of $ABO_{3-\delta}$ ($0 < \delta < 0.5$)

Consider a simple non-stoichiometric perovskite-type oxide, $ABO_{3-\delta}$, (*e.g.* A = Ln or Ae and B = M) with oxygen vacancies and valence defects on the B sub-lattice as the only defects. We will assume that A is a cation like Sr^{2+} or La^{3+}, which is not involved in the redox reactions, whereas B is a transition metal cation present in two oxidation states, B^{3+} and B^{4+} or B^{2+} and B^{3+}. Using the latter case, all the B atoms are trivalent for $\delta = 0$ (*i.e.* in ABO_3) and divalent for $\delta = 0.5$ (*i.e.* in $ABO_{2.5}$). We disregard any effect of intrinsic disorder, of ionic or electronic type. The removal of oxygen atoms results in the reduction of B atoms and for many systems this can be expressed in terms of a defect chemical reaction according to[5]

$$2O_O^x + 4B_B^x = 2V_O^{\bullet\bullet} + 4B'_B + O_2(g) \quad (1)$$

The corresponding equilibrium constant is given by

$$K = \frac{[V_O^{\bullet\bullet}]^2[B'_B]^4}{[O_O^x]^2[B_B^x]^4} \cdot pO_2(g) \quad (2)$$

and the oxygen pressure which corresponds to a certain value of δ is

$$\log pO_2(g) = \log K + 4\{\log(1-2\delta) - \log(2\delta)\} - 2\log\left(\frac{\delta}{3-\delta}\right) \quad (3)$$

For thermochemical uses, an expression for the integral Gibbs energy of formation of the compound $ABO_{3-\delta}$ is also needed. Such an expression can be derived by integration of eqn. (3) but in order to show clearly some of the main implications of the model a more detailed analysis starting from the partition function is preferred.

In the isobaric–isothermal (NPT) ensemble the partition

DOI: 10.1039/b106422n

function for a closed system is given by[6]

$$Z=\sum_{c}\sum_{s}\exp\left(-\frac{H_{c,s}}{kT}\right)=\sum_{c}\exp\left(-\frac{G_{c}}{kT}\right) \quad (4)$$

The summation over the enthalpy, $H_{c,s}$, is running over all the vibrational states, s, for all the different atomic configurations, c, of the system. The summation over the enthalpy for a particular atomic configuration is related to the Gibbs energy of that particular configuration, G_c, and the total partition function, Z, is given as the summation of the Gibbs energy of all the different atomic configurations of the system.

The Gibbs energy of formation of a compound with a given composition can now be derived by summation over all configurations that have a certain Gibbs energy of formation, $\Delta_f G_{c'}$, and an associated degeneracy, $g_{c'}$.

$$\Delta_f G=-kT\ln Z=-kT\ln\sum_{c'}g_{c'}\exp\left(-\frac{\Delta_f G_{c'}}{kT}\right) \quad (5)$$

The configurational entropy term, given by the degeneracy $g_{c'}$ is included in $\Delta_f G$ but not in $\Delta_f G_{c'}$.

Let us assume the existence of two compounds with different formal oxidation states for the B atom, ABO_3 and $ABO_{2.5}$. The two compounds have the same (perovskite-type) structure, and the non-stoichiometric phase $ABO_{3-\delta}$ is seen as a solution of these two 'limiting compounds'. Often only one of the limiting compounds is physically realizable. If we use the $LaMnO_{3-\delta}$ system where δ_{max} at 1473 K is near 0.053[7] as an example: $LaMnO_3$ can be made in the laboratory, but $LaMnO_{2.50}$ cannot. In other cases a complete solid solution exists and $SrFeO_{3-\delta}$ serves as an example where wide non-stoichiometry is observed at high temperatures.[8]

If we assume that the non-stoichiometric $ABO_{3-\delta}$ can be described as an ideal solution of the two limiting compounds ABO_3 and $ABO_{2.5}$, all configurations with a certain composition have the same Gibbs energy of formation since there are no defect–defect interactions. The Gibbs energy of formation of a configuration, $\Delta_f G_{c'}$, is, for a certain composition, given as

$$\begin{aligned}\Delta_f G_{c'}(ABO_{3-\delta})=&(1-2\delta)\Delta_f G^{o}(ABO_3)\\&+2\delta\Delta_f G^{o}(ABO_{2.5})\end{aligned} \quad (6)$$

The pure elements at 1 bar and at a particular temperature are chosen as standard state. Since all configurations with a given composition have the same Gibbs energy of formation, the total Gibbs energy of formation of a material with a specific composition is given by taking the number of configurations for that composition into consideration. In the ideal solution approach a random distribution of the different species on the different sub-lattices is assumed. Let us assume that oxygen atoms and oxygen vacancies on the oxygen sub-lattice and B^{2+} and B^{3+} on the B sub-lattice are randomly distributed. In this case, the degeneracy, $g_{c'}$, is

$$g_{c'}=\frac{(3N)!}{N_{V_O}!(3N-N_{V_O})!}\cdot\frac{N!}{N_{B^{2+}}!(N-N_{B^{2+}})!} \quad (7)$$

where N is the number of B atoms, N_{V_O} is the number of oxygen vacancies and $N_{B^{2+}}$ is the number of B^{2+} in $ABO_{3-\delta}$.

By substitution of eqns. (6) and (7) in eqn. (5) an expression for the total Gibbs energy of formation of the oxide in the ideal solution approximation is obtained.

$$\begin{aligned}\Delta_f G(ABO_{3-\delta})=&(1-2\delta)\Delta_f G^{o}(ABO_3)\\&+2\delta\Delta_f G^{o}(ABO_{2.5})\\&+RT\Big[(1-2\delta)\ln(1-2\delta)+2\delta\ln(2\delta)\\&+\delta\ln\left(\frac{\delta}{3}\right)+(3-\delta)\ln\left(1-\frac{\delta}{3}\right)\Big]\end{aligned} \quad (8)$$

Here, $\Delta_f G^{o}(ABO_{2.5})$ is the standard Gibbs energy of formation of each of all possible configurations of perovskite-type $ABO_{2.5}$. The fact that we have a number of configurations with this Gibbs energy of formation gives rise to an additional contribution of configurational origin given in the square brackets. For $\delta = 0.5$ this term represents (in the present ideal solution approximation) the entropy connected with disordering of ordered $ABO_{2.5}$ giving a completely random distribution of oxygen atoms and oxygen vacancies on the oxygen sub-lattice. Hence, the total Gibbs energy of formation of an oxide with a certain composition is given as a sum of a non-configurational and a configurational term.

The chemical potential of oxygen can now be derived and the related quantity $\log p_{O_2}$ expressed as a function of δ

$$\begin{aligned}\log pO_{2(g)}=&\left(\frac{1}{RT\ln 10}\right)\{4\Delta_f G^{o}(ABO_3)\\&-4\Delta_f G^{o}(ABO_{2.5})\}\\&+4\{\log(1-2\delta)-\log(2\delta)\}\\&-2\log\left(\frac{\delta}{3-\delta}\right)\end{aligned} \quad (9)$$

The first term on the right-hand side is in this ideal solution approach given by the standard Gibbs energy of oxidation,

$$\begin{aligned}&4\Delta_f G^{o}(ABO_3)-4\Delta_f G^{o}(ABO_{2.5})\equiv\Delta_{ox}G^{o}\\&=\Delta_{ox}H^{o}-T\cdot\Delta_{ox}S^{o}\end{aligned} \quad (10)$$

which corresponds to the reaction

$$4ABO_{2.5}(\text{perovskite})+O_2(g)\rightarrow 4ABO_3(\text{perovskite}) \quad (11)$$

In the ideal solid solution model used the enthalpy and entropy of oxidation are independent of composition. Non-ideal terms can easily be incorporated into the model. This will enable us to take compositional effects on the Gibbs energy of oxidation into consideration, and the Gibbs energy of oxidation will no longer be directly related to eqn. (11).

Both the reduced and the oxidized compounds in eqn. (11) are of the same structure, *e.g.* of the perovskite-type, and the corresponding enthalpy of formation of $ABO_{2.5}$ is the enthalpy of formation of a disordered phase with many possible configurations which all have the same enthalpy of formation (the ideal solution approach). With regard to the redox entropy it should be noted that the last two terms in eqn. (9) represent the partial configurational entropy of oxygen. Hence, the entropic contribution to the Gibbs energy of the redox reaction eqn. (11) should not include the structural configurational contribution since this term is included explicitly in the configurational part of the equation. Thus, when comparing calorimetric entropies with entropies deduced from equilibration studies, the configurational entropy should be subtracted from the calorimetric entropy.

In the preceding treatment we have assumed one defect reaction only [eqn. (1)] and the electronic defects are assumed to be localized. Intrinsic defects in the two compounds $ABO_{2.5}$ and ABO_3 are neglected. Eqn. (9), derived from the partition function, and eqn. (3), obtained using the Kröger–Vink approach, are identical. This implies that the right-hand side of eqn. (2) is indirectly an expression for the partial configurational entropy, whereas the left-hand side, the equilibrium constant, is given by

$$\log K=\left(\frac{1}{RT\ln 10}\right)\cdot\left(4\Delta_f G^{o}(ABO_3)-4\Delta_f G^{o}(ABO_{2.5})\right) \quad (12)$$

An alternative approach to this type of solution modeling is based on virtual potentials and structural building units; see, for example, Kröger *et al.*[9] and Schottky.[10]

Redox energetics of perovskite-related oxides

From enthalpies of oxidation to redox properties and *vice versa*

The ideal solution model allows us to describe the redox properties of perovskite-type oxides provided that the enthalpy of oxidation [eqns. (10) and (11)] is known. The corresponding entropy has a smaller influence (varies less) on the redox properties and is assumed to be $-130\ \mathrm{J\ K^{-1}\ mol\ O_2^{-1}}$. Figs. 1 and 2 compare experimental (composition, P_{O_2}, T)-relationships and model calculations using composition-independent enthalpies of oxidation determined calorimetrically. Composition–partial-pressure isotherms for $La_{1-x}Ca_xCrO_{3-\delta}$[11,12] and $La_{1-x}Sr_xCrO_{3-\delta}$[13] are shown in Fig. 1 whereas the variation of the stoichiometry of cubic $SrMnO_{3-\delta}$[14,15] and of $CaMnO_{3-\delta}$[4] in air with temperature is shown in Fig. 2. The overall agreement is good and the calorimetrically determined enthalpies of oxidation and the partial thermodynamic quantities measured by equilibration methods are consistent. Some details are not reproduced by the calculations and the need of more complex models than the presently used ideal solution model is indicated. A short discussion is given below.

Eqns. (8) and (9) suggest that the redox behavior of a material is given by the relative stability of the different oxidation states involved. In this respect the crystal structure of the material is important; both the reduced and the oxidized compounds in eqns. (8) and (9) are of the same structure. The significance of this argument is illustrated through the redox properties of hexagonal and cubic $SrMnO_{3-\delta}$.[4] The oxygen stoichiometry of these two phases in air is given as a function of temperature in Fig. 3. The large difference in temperature for the calculated initial reduction in air, *ca.* 700 K for the cubic phase *versus ca.* 1300 K for hexagonal $SrMnO_{3-\delta}$, may at first sight seem strange since the enthalpy difference between the cubic and hexagonal modification of $SrMnO_3$ is only about 6 kJ mol^{-1}.[16] However, the temperature of initial reduction is given by the difference in Gibbs energy between the oxidized and reduced limiting compounds of the solid solution. And while cubic $SrMnO_{2.5}$ is relatively stable (can be prepared in the laboratory),[17] hexagonal $SrMnO_{2.5}$ is unstable. The Gibbs energy difference between the oxidized and reduced compounds is, hence, much larger for the hexagonal case than for the cubic case. The reason for this can be understood by taking the structure of hexagonal $SrMnO_3$ into consideration.[18] While the Mn–O_6 octahedra share corners in the usual cubic perovskite-type structure, they share faces in the hexagonal structure (see Fig. 4). Reduction of the cubic structure gives

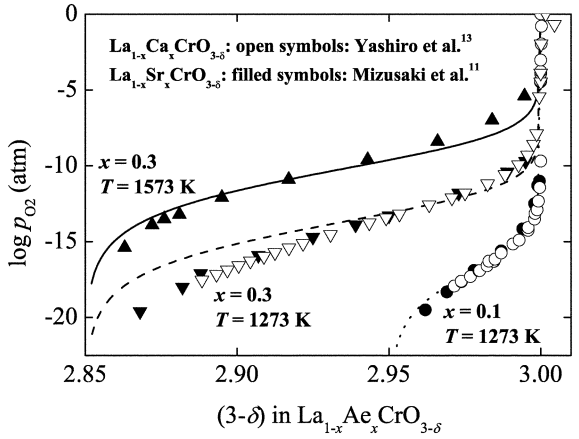

Fig. 1 $(3-\delta)$ in $La_{1-x}Ae_xCrO_{3-\delta}$ as a function of T and P_{O_2}. References to the experimental points are given in the figure. The lines are calculated using the ideal solution model with calorimetrically determined average enthalpies of oxidation and an estimated entropy of oxidation. For further details see Stølen *et al.*[12]

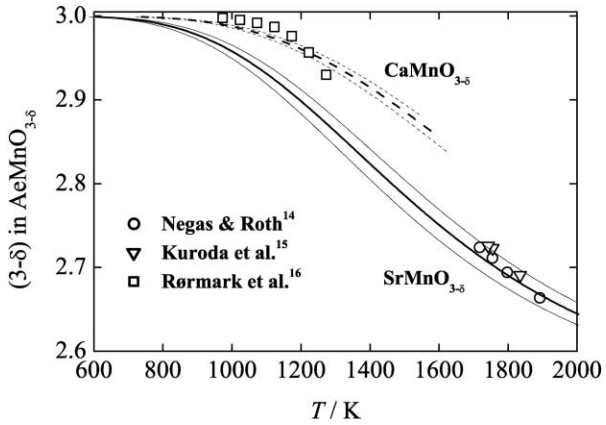

Fig. 2 $(3-\delta)$ for cubic $AeMnO_{3-\delta}$ in air as a function of T. References to the experimental points are given in the figure. The lines are calculated using the ideal solution model with calorimetrically determined average enthalpies of oxidation and an estimated entropy of oxidation. $\Delta_{ox}H(SrMnO_{3-\delta}) = -293 \pm 10\ \mathrm{kJ\ mol\ O_2^{-1}}$; $\Delta_{ox}H(CaMnO_{3-\delta}) = -356 \pm 7\ \mathrm{kJ\ mol\ O_2^{-1}}$. The three lines represent in each case the best value (the thick line) and the estimated uncertainty (the thin lines).

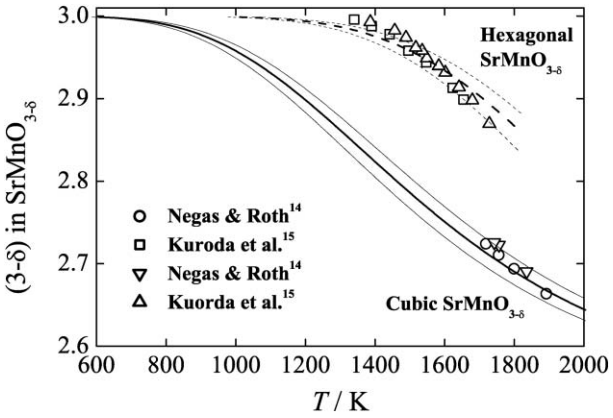

Fig. 3 $(3-\delta)$ for cubic and hexagonal $SrMnO_{3-\delta}$ in air as a function of T. References to the experimental points are given in the figure. The lines for the cubic phase are calculated using the ideal solution model with the calorimetrically determined average enthalpy of oxidation and an estimated entropy of oxidation. $\Delta_{ox}H(SrMnO_{3-\delta}, \mathrm{cub}) = -293 \pm 10\ \mathrm{kJ\ mol\ O_2^{-1}}$; for the hexagonal case $\Delta_{ox}H(SrMnO_{3-\delta}, \mathrm{hex}) = -590 \pm 20\ \mathrm{kJ\ mol\ O_2^{-1}}$ and $\Delta_{ox}S = -230\ \mathrm{J\ K^{-1}\ mol\ O_2^{-1}}$ is used. The three lines represent in each case the best value (the thick line) and the estimated uncertainty (the thin lines).

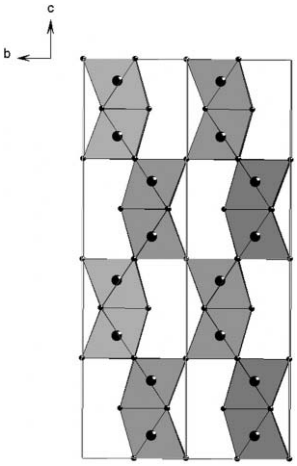

Fig. 4 Polyhedron description of the crystal structure of hexagonal $SrMnO_3$.[18] Large symbols represent manganese atoms, small symbols oxygen atoms. Mn–O_6 octahedra are given in grey.

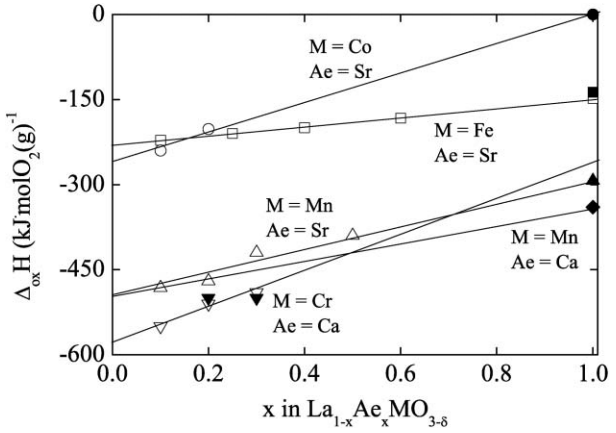

Fig. 5 Enthalpy of oxidation of $La_{1-x}Ae_xMO_{3-\delta}$ as a function of x. Open symbols represent values deduced using equilibrium data from literature. Closed symbols are calorimetrically determined values. $La_{1-x}Sr_xCoO_{3-\delta}$: ○, Mizusaki *et al.*[27] and Lankhorst *et al.*;[25] ●, Evenrud.[26] $La_{1-x}Sr_xFeO_{3-\delta}$: □, Mizusaki *et al.*[19,20] and Holt *et al.*;[21] ■, Haavik *et al.*[22] $La_{1-x}Sr_xMnO_{3-\delta}$: △, Kuo *et al.*[23] and Mizusaki *et al.*;[24] ▲, Rørmark *et al.*[4] $La_{1-x}Ca_xMnO_{3-\delta}$: ◆, Rørmark *et al.*[4] $La_{1-x}Ca_xCrO_{3-\delta}$: ▽, Yashiro *et al.*;[11] ▼, Stølen *et al.*[12]

rise to square pyramidal coordinated manganese whereas reduction of the hexagonal structure in the end probably would lead to face-shared octahedra separated by planes with high oxygen-vacancy concentration. The latter structure must be expected to be energetically unfavorable. In conclusion, the redox energetics of a phase depend strongly upon the crystal structure, a fact that should be taken into account when looking for trends in redox properties.

The present ideal solution model with $\Delta_{ox}H$ independent of oxygen stoichiometry may seem like an oversimplification for complex oxides like the perovskite-related ones. However, the simplicity of the model allows us to deduce trends in the redox energetics. Enthalpies of oxidation can be deduced from stoichiometry–partial-pressure curves by using an estimated entropy of oxidation, in our case chosen to be $-130\ \mathrm{J\ K^{-1}\ mol\ O_2{}^{-1}}$. Here, it is important to note that the composition–partial-pressure range close to the fully oxidized compound preferably is used for evaluation of the enthalpy of oxidation. In this compositional region, effects of defect–defect interactions are less important. The obtained enthalpy of oxidation[11–13,19–27] of M(III) to M(IV) for $La_{1-x}Ae_xMO_{3-\delta}$ is plotted as function of x in Fig. 5. Calorimetrically determined enthalpies are also included and it is reassuring to see that the enthalpy of oxidation of $La_{1-x}Ae_xMO_{3-\delta}$ deduced from equilibrium studies extrapolates to the calorimetrically determined enthalpies of oxidation of $SrMnO_{3-\delta}$,[4] $SrFeO_{3-\delta}$[22] and $SrCoO_{3-\delta}$.[26]

Hence, $\Delta_{ox}H$ varies to a first approximation linearly with composition x for $La_{1-x}Ae_xMO_{3-\delta}$. A numerical description is given in Table 1. The agreement between experimental composition–partial-pressure isotherms and calculated curves using the tabulated enthalpy equations, illustrated in Fig. 6, is largely good. The deviation observed for $La_{0.7}Sr_{0.3}MnO_{3-\delta}$ for large δ is due to decomposition of the oxide.[24] This does not

Table 1 Enthalpy of oxidation of M(III) to M(IV) in kJ mol $O_2{}^{-1}$

Tm	Binary oxide MO/M_2O_3	$La_{1-x}Sr_xMO_{3-\delta}$	$La_{1-x}Ca_xMO_{3-\delta}$
Cr	−112		−577 + 300x
Mn	−160	−499 + 210x	−499 + 143x
Fe	110	−231 + 82x	
Co	180	−261 + 261x	

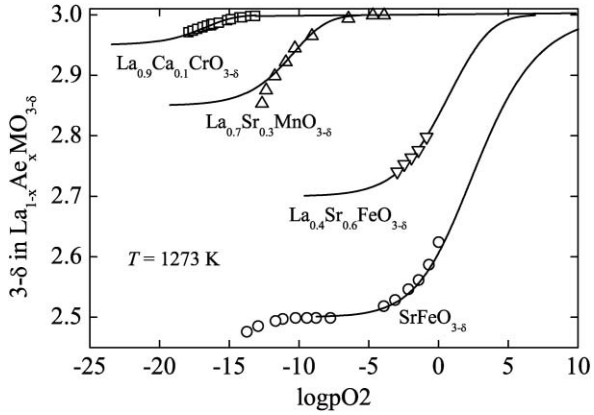

Fig. 6 $(3-\delta)$ in $La_{1-x}Ae_xMO_{3-\delta}$ at 1273 K as a function of P_{O_2}. Experimental data: □, Yashiro *et al.*;[13] △, Mizusaki *et al.*;[24] ▽, Mizusaki *et al.*;[19] ○, Holt *et al.*[21] The lines are calculated values using enthalpies of oxidation deduced from Table 1.

affect the evaluation of the energetics of eqn. (9) that dominate when δ is small.

The present evaluation suggests that the enthalpy of oxidation is a linear function of x in $La_{1-x}Ae_xMO_{3-\delta}$ and furthermore is independent of δ. Earlier calorimetric studies of the enthalpy of oxidation of K_2NiF_4-type $La_{2-x}Sr_xCuO_{4-\delta}$[28] and $La_{2-x}Sr_xCoO_{4-\delta}$[29] suggest that the enthalpy of oxidation is independent of x whereas a study of $BaNiO_{2+\delta}$ suggests an independence of δ.[30] Furthermore, the entropy of oxidation of $SrFeO_{3-\delta}$ has recently been shown to be independent of δ.[31] Enthalpies and entropies of oxidation that are dependent of the oxygen stoichiometry are on the other hand suggested from equilibration studies of $La_{2-x}Sr_xCuO_{3-\delta}$[32] and $La_{0.8}Sr_{0.2}CoO_{3-\delta}$.[2] In conclusion, the ideal solution behavior seems to be a reasonable approach although deviations from this ideal behavior must be expected in some cases. This topic is discussed to some extent below.

Entropic contributions to the redox energetics

The enthalpy of oxidation has larger influence on the redox properties than the corresponding entropy of oxidation. Still, values used for the entropy of a reaction that consumes one gas molecule, typically $-130\ \mathrm{J\ K^{-1}\ mol^{-1}}$, should be considered only as rough estimates. The entropy of oxidation values[33] of selected transition metal monoxides to sesqui-oxides according to

$$\mathrm{MO(s)} + 1/4\mathrm{O_2(g)} = 1/2\mathrm{M_2O_3(g)} \qquad (13)$$

and of selected sesqui-oxides to dioxides are given as a function of temperature in Fig. 7. Two main features are obvious. The entropy of oxidation varies greatly from case to case and significantly with temperature. The entropy difference between product and reactant is obviously of great importance. Let us use $SrFeO_{3-\delta}$ as an example. The entropy of oxidation, given by the difference in entropy between $SrFeO_{2.5}$ and $SrFeO_3$, can be deconvoluted into approximate vibrational, electronic and magnetic contributions. If we use $T = 1000$ K as an example, $SrFeO_{2.5}$ is structurally ordered but magnetically disordered. Using an estimated magnetic entropy based on the spin-only approximation were $\Delta_{magn}S$ is given by $R\ln(2S+1)$, the total harmonic + anharmonic vibrational entropy can be deduced[31] (see Fig. 8). The electronic contribution is negligibly small for semi-conducting $SrFeO_{2.5}$. $SrFeO_3$ is, on the other hand, reported to have metallic conductivity[7] and a significant electronic heat capacity coefficient must be expected. Let us assume an electronic heat capacity coefficient of the order observed for metals, $5\ \mathrm{mJ\ K^{-1}\ mol^{-1}}$. Using the spin-only magnetic entropy the total vibrational entropy is obtained.

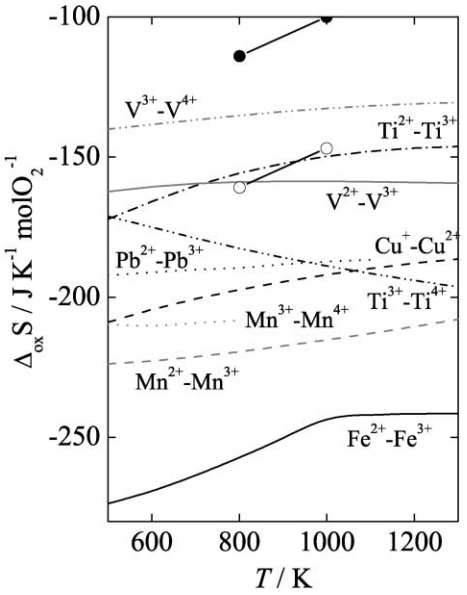

Fig. 7 Entropy of oxidation per mole of O_2 as a function of temperature. The value for $SrFeO_{3-\delta}$ is compared with values for pairs of binary transition metal oxides (the thermochemical data are taken from Barin[33]). Example: Ti^{3+}–Ti^{4+} represent the reaction $2Ti_2O_3 + O_2(g) = 4TiO_2$. The entropy of oxidation of brownmillerite-type $SrFeO_{2.5}$ (●) and of perovskite-type $SrFeO_{2.5}$ (○) to perovskite-type $SrFeO_{2.833}$ are also given.[31]

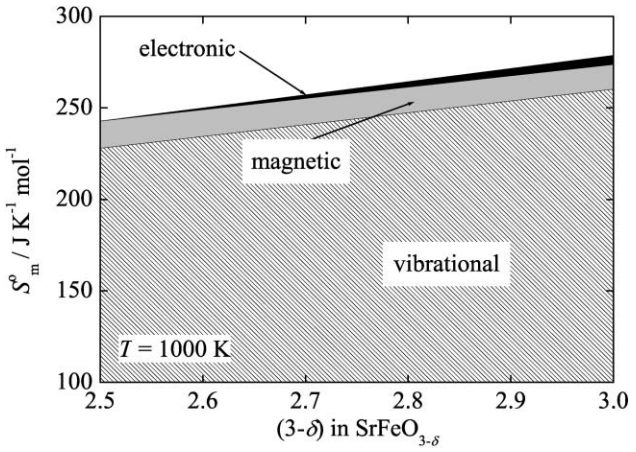

Fig. 8 Deconvolution of the non-configurational entropy of $SrFeO_{2.5}$ and of $SrFeO_3$ at 1000 K into contributions of vibrational, magnetic and electronic origin. See text for further explanation.

Although this deconvolution scheme is uncertain a main conclusion is evident; the entropic contribution to the redox energetics is to a large extent given by the vibrational entropies of the limiting compounds, in this case $SrFeO_{2.5}$ and $SrFeO_3$. Fig. 7 shows that the vibrational properties are important also for the entropy of oxidation of binary transition metal oxides. The main reason for the large spread in $\Delta_{ox}S$ is related to large variations in the vibrational characteristics of the different binary oxides. It follows that the entropic contribution to the redox energetics of ternary non-stoichiometric oxides also must be expected to vary considerably from case to case.

While the absolute values of the entropy[33] of the binary iron oxides FeO and Fe_2O_3 are approximately equal per mole of iron, the entropy of $SrFeO_{3-\delta}$ shows a much stronger dependence on composition.[33] A main difference is that whereas, for instance, FeO and Fe_2O_3 take different structures, the changes in structure on going from $SrFeO_{2.5}$ to $SrFeO_3$ are much smaller. Hence, to a first approximation the entropy of $SrFeO_{3-\delta}$ depends on the total number of atoms present in the compound. New atoms that are incorporated into the structure do not alter the vibrational characteristics of the phase significantly but contribute with six degrees of freedom per atom, hence by a $3k$ contribution to the heat capacity at high temperatures.

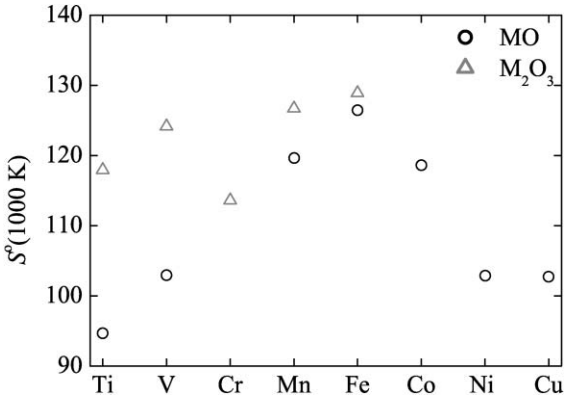

Fig. 9 Standard entropy of first row transition metal monoxides and sesqui-oxides at 1000 K per mol M.[33]

On the other hand, while the entropy values of FeO and Fe_2O_3 are almost equal per mole of iron, a large difference is observed between the entropy values of TiO and Ti_2O_3. The entropy of selected binary transition metal oxides at 1000 K is given in Fig. 9. The vibrational characteristics of a compound are in general given by the structure/electron band structure, and the difference in behavior between the FeO/Fe_2O_3 and TiO/Ti_2O_3 pairs seems to relate to differences in electronic band structure that affect the cohesive properties of the compounds and, hence, the vibrational characteristics. Fig. 10 shows the average Tm–O distances[34] for the first coordination sphere of monoxides and sesqui-oxides of the first series of the transition elements. Both the transition metal–oxygen distance and the entropy of the monoxides show the same general trend; both properties increase from Ti to Mn and Fe and then decrease. For the sesqui-oxides neither the Tm–O distances nor the entropy varies much with Tm. The small difference in entropy between FeO and 1/2 Fe_2O_3 relative to the difference between TiO and 1/2 Ti_2O_3, hence, seem to be related to bond strength. The average Fe–O distance is about 7% larger for FeO compared with Fe_2O_3 whereas it is 3.5% larger for TiO relative to Ti_2O_3. The long Fe–O distances in FeO indicate a low Debye temperature and, hence, high entropy. This is the primary reason for the different behavior of the iron *versus* the titanium oxides. This sort of indirect electronic contribution to the redox entropy must be taken into account to understand fully the entropic contribution to the redox energetics. Large differences in the entropic contribution to the redox energetics may be expected from one system to another.

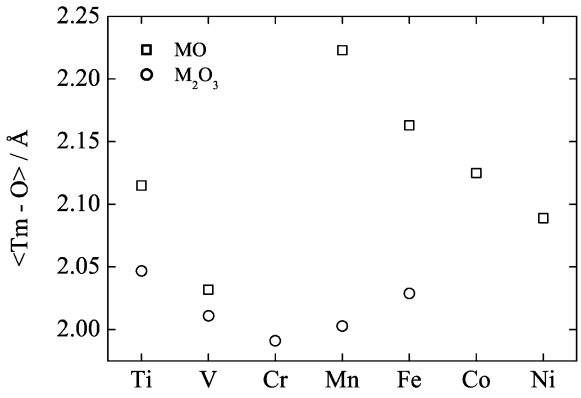

Fig. 10 Average shortest metal–oxygen distance in first row transition metal monoxides and sesqui-oxides.[34]

Alternative models and correlations

The slope of the observed non-stoichiometry of $CaMnO_{3-\delta}$ in air *versus* temperature[4] is steeper than predicted by the model (see Fig. 2) and the deviations are even more pronounced for hexagonal $SrMnO_{3-\delta}$[4,14,15] (Fig. 3). There may be several reasons for this behavior and additional features must be included in the model.

In cases where the enthalpy of oxidation is known from calorimetry (as is the case for $CaMnO_{3-\delta}$[4]), the entropy of oxidation may be used as a parameter that can be adjusted within reason to fit the observed equilibrium data. Furthermore, the heat capacity of reaction (11) and, hence, the variation of the enthalpy and entropy of oxidation with temperature can be taken into account. The effect of these adjustments is, however, not large and does not give a significantly increased agreement between experimental points and model calculations in the present cases.

Two other reasons for the deviations are easily suggested. In the first we let the enthalpy of oxidation, $\Delta_{ox}H^{o}$, vary to some degree with composition as is expected and suggested by others.[2] In the other we suggest alternative models for the configurational entropy. The variation of $\Delta_{ox}H$ with composition may be taken into account by including a defect–defect interaction term, Ω. We prefer to use a defect–defect interaction term on the oxygen sub-lattice and suggest this term to be proportional to the probability of finding two oxygen vacancies next to each other. The Gibbs energy of $ABO_{3-\delta}$ is in this approach given as[35]

$$\begin{aligned}\Delta_f G(ABO_{3-\delta}) = {} & (1-2\delta)\Delta_f G^{o}(ABO_3) \\ & + 2\delta\Delta_f G^{o}_{H}(ABO_{2.5}) \\ & + \frac{\delta^2}{6}\Omega + RT\left[(1-2\delta)\ln(1-2\delta)\right. \\ & \left. + 2\delta\ln(2\delta) + \delta\ln\left(\frac{\delta}{3}\right) + (3-\delta)\ln\left(1-\frac{\delta}{3}\right)\right]\end{aligned} \quad (14)$$

$\Delta_f G_H{}^{o}(ABO_{2.5})$ here refers to Henryan $ABO_{2.5}$ obtained by extrapolation of the ideal Henryan behavior of $ABO_{3-\delta}$ for δ near zero to $\delta = 0.5$. The interaction term takes the deviation from the Henryan behavior at high defect concentrations into consideration. The equilibrium partial pressure of oxygen corresponding to a particular δ is now given as

$$\begin{aligned}\log pO_{2(g)} = {} & \left(\frac{1}{RT\ln 10}\right)\left\{4\Delta_f G^{o}(ABO_3)\right. \\ & \left. - 4\Delta_f G^{o}_{H}(ABO_{2.5}) - \frac{2\delta}{3}\cdot\Omega\right\} \\ & + 4(\log(1-2\delta) - \log(2\delta)) \\ & - 2\log\left(\frac{\delta}{3-\delta}\right)\end{aligned} \quad (15)$$

The first term on the right-hand side is in this approach the non-configurational Gibbs energy of oxidation[35]

$$\begin{aligned}& 4\Delta_f G^{o}(ABO_3) - 4\Delta_f G^{o}_{H}(ABO_{2.5}) - \frac{2\delta}{3}\cdot\Omega \\ & \equiv \Delta_{ox}G(\delta) = \Delta_{ox}H(\delta) - T\cdot\Delta_{ox}S(\delta)\end{aligned} \quad (16)$$

If Ω is assumed to be temperature-independent, the model corresponds to a 'regular solution' model and the excess contribution is purely enthalpic. The enthalpy of oxidation is in this approach not directly related to a reaction of the form as in reaction (11) but a function of δ in $ABO_{3-\delta}$.

The stoichiometry of $CaMnO_{3-\delta}$ in air is given as a function of temperature in Fig. 11.[16] The solid curve calculated using the calorimetrically determined enthalpy of oxidation[4] (-356 kJ mol^{-1}) and $\Delta_{ox}S = -130$ J K^{-1} mol^{-1} shows a significantly different behavior to that of the experimental data. Much better agreement is obtained by using the regular solution model with the constriction that the average enthalpy of oxidation should be equal to the calorimetrically determined average one. The variation of the enthalpy of oxidation with composition for the regular solution approach is in Fig. 12 compared with the average enthalpies of oxidation obtained by high-temperature calorimetry. Experimental values for two different compositional regions, $0.47 < \delta < 0.0$ and $0.23 < \delta < 0.0$, are shown. A free fit using the regular solution model gives better agreement with the experimental stoichiometry–temperature data (Fig. 11) but suggests that the oxidation becomes more exothermic when δ in $CaMnO_{3-\delta}$ decreases (see Fig. 12). This behavior is not in agreement with the calorimetric values that may be taken to suggest that the oxidation becomes less exothermic when the non-stoichiometry decreases.

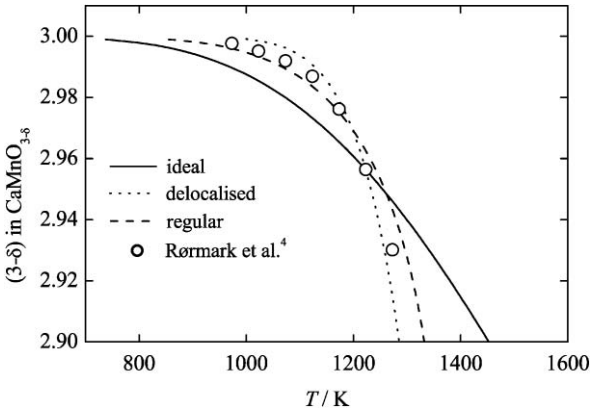

Fig. 11 $(3-\delta)$ for $CaMnO_{3-\delta}$ in air as a function of T. ○, Rørmark *et al.*[16] Solid line, ideal solution model with random distribution of oxygen atoms and oxygen vacancies on the oxygen sub-lattice and Mn^{3+} and Mn^{4+} at the manganese sub-lattice. Dotted line, 'delocalised' electron model with random distribution of oxygen atoms and oxygen vacancies on the oxygen sub-lattice – no contribution from the electrons on the B sub-lattice. These electrons are either delocalised or strongly coupled to the vacancies. In both these cases $\Delta_{ox}H(CaMnO_{3-\delta}) = -356$ kJ mol $O_2{}^{-1}$. Dashed line, regular solution model. The average enthalpy of oxidation is constricted to be equal to that determined by calorimetry, -356 kJ mol $O_2{}^{-1}$.

With regard to models based on alternative descriptions of the configurational entropy, the steepness of the experimental $(3-\delta)$ *versus* T curve (Fig. 11) is consistent with a smaller configurational entropy relative to that of eqns. (8) and (14).

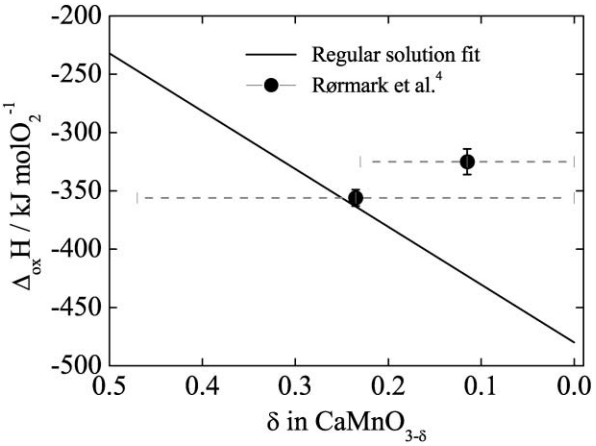

Fig. 12 Comparison of the compositional dependence of the enthalpy of oxidation resulting from a free fit to the experimental non-stoichiometry data[16] using the regular solution model, and experimental determinations. The two calorimetric data points represent average enthalpies of oxidation determined for a compositional range as indicated by the bars on the x-axis.[4]

This is either due to clustering of some kind or is due to a delocalized character of the electrons. In eqns. (8) and (9) configurational terms that correspond to complete disorder both on the O and B sub-lattices are included; *i.e.* a random mixture of oxygen vacancies and oxygen atoms and of the transition metal atom in two different oxidation states is assumed for the O and B sub-lattices, respectively. Configurationally averaged lattice energy simulations indicate a significant order in terms of the presence of transition metal octahedra, square pyramids and tetrahedra in non-stoichiometric perovskites and suggest that the disordered structures should be described in terms of these structural entities.[36] Hence, the structural entities often observed in low temperature superstructures are preserved even at high temperatures.[36] This will clearly reduce the configurational entropy but mathematical expressions taking care of such reduced disorder correctly are not available. Also the assumption of localized electrons that result in transition metal atoms present in two different well-defined oxidations states is questionable. Alternative models can be constructed. One simple possibility is obtained by assuming that the electrons are completely delocalized (with no electronic entropy). Alternatively, the electrons can be assumed to be strongly coupled to the oxygen vacancies. Both these models give the same configurational entropy and allow a reasonable description of the observed non-stoichiometry data when using the calorimetric average enthalpy of oxidation (see Fig. 11).

Since the non-stoichiometry is known for a rather limited temperature range only, the data do not allow us to discriminate between the different models that give approximately the same agreement with experiments. In all the modeling of $CaMnO_{3-\delta}$ the calorimetric value for the enthalpy of oxidation has been used. The use of a free-fit approach to the experimental data gives significantly different enthalpies of oxidation. Hence, directly measured enthalpies of oxidation give highly valuable constrictions in the modeling of non-stoichiometry data. Calorimetrically determined partial enthalpies of oxidation would be even more valuable and should be a primary goal for further studies.

Summary

A thermodynamic model that describes the redox energetics of non-stoichiometric perovskite-related oxides has been presented, in which the redox properties are rationalized in terms of the relative stability of the oxidation states involved. A number of systems considered can be adequately described with an enthalpy of oxidation that is independent of oxygen stoichiometry. The stability of a given oxidation state is related to the structure of the oxide, and the large difference in redox behavior between hexagonal and cubic $SrMnO_{3-\delta}$ has been discussed. Enthalpies of oxidation obtained directly by calorimetry and indirectly from equilibrium data are consistent, and the combined data show that the enthalpy of oxidation of selected $La_{1-x}Ae_xMO_{3-\delta}$ phases varies linearly with x. While the entropy of oxidation is a less important contribution to the Gibbs energy of the reactions considered, it varies considerably from one system to another. The variations are largely related to the vibrational characteristics of the phases. Further studies are needed to understand these variations. More complex models that may be applicable in cases where the simpler model fails are discussed. Discrimination between the different models may constitute a problem in cases were equilibrium data are available for a limited compositional region only. Calorimetrically determined enthalpies of oxidation will in these cases give highly valuable constrictions in the modeling of the non-stoichiometry data.

Acknowledgement

Support from NFR is acknowledged.

References

1 J. Mizusaki, M. Yoshihiro, S Yamauchi and K. Fueki, *J. Solid State Chem.*, 1987, **67**, 1.
2 M. H. R. Lankhorst, H. J. M. Bouwmeester and H. Verweij, *J. Am. Ceram. Soc.*, 1997, **80**, 2175.
3 A. Navrotsky, *Pure Appl. Chem.*, 1994, **66**, 1759.
4 L. Rørmark, A. B. Mørch, K. Wiik, S. Stølen and T. Grande, *Chem. Mater*, 2001, **13**, 4005.
5 F. A. Kröger, *The Chemistry of Imperfect Crystals*, North-Holland, Amsterdam, 1974.
6 N. L. Allan, G. D. Barrera, R. M. Fracchia, M. Yu. Lavrentiev, M. B. Taylor, I. T. Todorov and J. A. Purton, *Phys. Rev. B*, 2001, **6309**, 4203.
7 K. Kamata, T. Nakajima, T. Hayashi and T. Nakamura, *Mater. Res. Bull.*, 1978, **13**, 49.
8 Y. Takeda, K. Kanno, T. Takada, O. Yamamoto, M. Takano, N. Nakaya and Y. Bando, *J. Solid State Chem.*, 1986, **63**, 237.
9 F. A. Kröger, F. H. Stieltjes and H. J. Vink, *Philips Res. Rep.*, 1959, **14**, 557.
10 W. Schottky, *Z. Elektrochem.*, 1939, **45**, 33.
11 K. Yashiro, S. Onuma, S. Miyoshi, A. Kaimai, K. Kawamura, Y. Nigara, T. Kawada, J. Mizusaki, N. Sakai and H. Yokokawa, The American Ceramic Society 103rd Annual Meeting and Exposition, Abstract book (2001) 145, Indianapolis, IN, USA.
12 S. Stølen, N. Sakai and E. Bakken, *J. Therm. Anal. Calor.*, 1999, **57**, 823.
13 J. Mizusaki, S. Yamauchi, K. Fueki and A. Ishikawa, *J. Solid State Chem.*, 1984, **12**, 119.
14 T. Negas and R. S. Roth, *J. Solid State Chem.*, 1970, **1**, 409.
15 K. Kuroda, K. Shinozaki, K. Uematsu, N. Mizutani and M. Kato, *J. Am. Ceram. Soc.*, 1980, **63**, 109.
16 L. Rørmark, K. Wiik, S. Stølen and T. Grande, *J. Mater. Chem.*, in press.
17 V. Caignaert, N. Nguyen, M. Hervieu and B. Raveu, *Mater. Res. Bull.*, 1985, **20**, 479.
18 K. Kuroda, N. Ishizawa, N. Mizutani and M. Kato, *J. Solid State Chem.*, 1981, **38**, 297.
19 J. Mizusaki, M. Yoshihiro, S. Yamauchi and K. Fueki, *J. Solid State Chem.*, 1985, **58**, 257.
20 J. Mizusaki, M. Yoshihiro, S. Yamauchi and K. Fueki, *J. Solid State Chem.*, 1987, **67**, 1.
21 A. Holt, T. Norby and R. Glenne, *Ionics*, 1999, **5**, 434.
22 C. Haavik, T. Atake and S. Stølen, *Phys. Chem. Chem. Phys.*, in press.
23 J. H. Kuo, H. U. Anderson and D. M. Sparlin, *J. Solid State Chem.*, 1989, **83**, 52.
24 J. Mizusaki, N. Mori, H. Takai, Y. Yonemura, H. Minamiue, H. Tagawa, M. Dokiya, H. Inaba, K. Naraya, T. Sasamoto and T. Hashimoto, *Solid State Ionics*, 2000, **129**, 163.
25 M. H. R. Lankhorst, H. J. M. Bouwmeester and H. Verweij, *J. Solid State Chem.*, 1997, **133**, 555.
26 H. Evenrud, Master Thesis, University of Oslo, 2000 (in Norwegian).
27 J. Mizusaki, Y. Mima, S. Yamauchi and K. Fueki, *J. Solid State Chem.*, 1989, **80**, 102.
28 J. Bularzik, A. Navrotsky, J. DiCarlo, J. Bringley, B. Scott and S. Trail, *J. Solid State Chem.*, 1991, **93**, 418.
29 T. R. S. Prasanna and A. Navrotsky, *J. Solid State Chem.*, 1994, **112**, 192.
30 J. DiCarlo, I. Yazdi, A. J. Jacobson and A. Navrotsky, *J. Solid State Chem.*, 1994, **109**, 223.
31 C. Haavik, T. Atake, H. Kawaji and S. Stølen, *Phys. Chem. Chem. Phys.*, 2001, **3**, 3863.
32 H. Kannai, J. Mizusaki, H. Tagawa, S. Hoshiyama, K. Hirano, K. Fujita, M. Tezuka and T. Hashimoto, *J. Solid State Chem.*, 1997, **131**, 150.
33 I. Barin, *Thermochemical Data of Pure Substances*. VCH, Verlagsgesellschaft mbH, Weinheim, 1993.
34 P. Villars and L. D. Calvert, *Pearson's Handbook of Crystallographic Data for Intermetallic Phases*, OH, USA, 2nd edn., 1991.
35 E. Bakken, T. Norby and S. Stølen, to be published.
36 E. Bakken, B. Pongsai, N. L. Allan and S. Stølen, to be published.